

Quarry Residue: Treatment of Industrial Effluent Containing Dye

Lariana Negrão Beraldo de Almeida ^{1,*}, Tatiana Gulminie Josué ², Othavio Henrique Lupepsa Nogueira ², Daniele Toniolo Dias ³ , Angelo Marcelo Tusset ⁴, Onélia Aparecida Andreo dos Santos ¹ and Giane Gonçalves Lenzi ²

¹ Departamento de Engenharia Química, Universidade Estadual de Maringá, 5790, Maringá 87020-900, Brazil; oaasantos@uem.br

² Departamento de Engenharia Química, Universidade Tecnológica Federal do Paraná, Rua Doutor Washington Subtil Chueire, 330, Ponta Grossa 84016-210, Brazil; tatianajosue@alunos.utfpr.edu.br (T.G.J.); othavionogueira@alunos.utfpr.edu.br (O.H.L.N.); gianeg@utfpr.edu.br (G.G.L.)

³ Departamento Acadêmico de Física, Universidade Tecnológica Federal do Paraná, Rua Doutor Washington Subtil Chueire, 330, Ponta Grossa 84016-210, Brazil; danieletdias@utfpr.edu.br

⁴ Departamento de Engenharia, Universidade Tecnológica Federal do Paraná, Rua Doutor Washington Subtil Chueire, 330, Ponta Grossa 84016-210, Brazil; tusset@utfpr.edu.br

* Correspondence: pg53631@uem.br or beraldolariana@gmail.com

Abstract: This work is devoted to the investigation of the discoloration of the synthetic and industrial effluent, using a quarry residue (MbP), which is a material naturally composed of mixed oxides, compared to zinc oxide (ZnO), acting as photocatalysts and adsorbents. The optimization of the pH and catalyst concentration parameters was carried out, and the industrial effluent was then treated by photocatalytic reactions, adsorption, and photolysis. Industrial effluent was supplied by a packaging company and was collected for a period of seven consecutive days, showing the oscillation of the parameters in the process. The material characterizations were obtained by scanning electron microscopy (SEM-EDS), X-Ray diffraction (XRD), and photoacoustic spectroscopy (PAS). The results indicated that the composition of the quarry waste is mainly silica and has E_{gap} 2.16 eV. The quarry residue as photocatalyst was active for the artificial effluent (synthetic dye solution), with a maximum of 98% discoloration, and as an adsorbent for industrial effluent, with a maximum of 57% of discoloration. Although the quarry residue has shown results lower than ZnO, it is considered a promising material in adsorption processes and photocatalytic reactions for discoloration of aqueous solutions.

Keywords: adsorption; photolysis; photocatalysis; quarry residue; discoloration; packaging industry



Citation: Almeida, L.N.B.d.; Josué, T.G.; Nogueira, O.H.L.; Dias, D.T.; Tusset, A.M.; Santos, O.A.A.d.; Lenzi, G.G. Quarry Residue: Treatment of Industrial Effluent Containing Dye. *Catalysts* **2021**, *11*, 852. <https://doi.org/10.3390/catal11070852>

Academic Editors: Gassan Hodaifa and Rafael Borja

Received: 10 June 2021

Accepted: 12 July 2021

Published: 16 July 2021

Publisher's Note: MDPI stays neutral with regard to jurisdictional claims in published maps and institutional affiliations.



Copyright: © 2021 by the authors. Licensee MDPI, Basel, Switzerland. This article is an open access article distributed under the terms and conditions of the Creative Commons Attribution (CC BY) license (<https://creativecommons.org/licenses/by/4.0/>).

1. Introduction

Dyes are chemical compounds that have the ability to color the surface of materials such as fabric fibers, packaging, and food. Industrial processes that use water and dyes in the production stages probably will present dye residual concentrations in effluent. Effluents, before being released into the environment or even reused, will need to undergo treatments to remove, among other compounds, their coloring.

Different techniques are performed to promote discoloration, including ultrafiltration, coagulation, flocculation, sonochemical decomposition, adsorption, biological treatments, heterogeneous photocatalysis, Fenton and photo-Fenton processes, advanced oxidation electrochemical processes, etc. [1–4].

Heterogeneous photocatalysis is classified as an advanced oxidative process [5] and has been widely studied due to its diversified application, such as the reduction of chromium VI to chromium III [6], mercury reduction [7], degradation of emerging pollutants such as caffeine [8], drugs [9,10], dyes [11], and reduction of bromate in water intended for human consumption [12].

In photocatalytic reactions, there are many variables that must be considered in order, such as the radiation source, pH of the reaction medium, temperature, and material used as a semiconductor material. The main materials used in the photoreactions are TiO_2 and ZnO as they are nontoxic and have good photochemical properties [13–16]; however, researchers commonly describe improvements in the catalysts' properties through new syntheses [17], the addition of metals [18,19], mixed oxides, etc.

In this direction, the search for new catalytic materials is also a very interesting and encouraging subject, particularly if this new material is a by-product in large quantities or a waste product without the exact destination of any industrial process.

The rice husk can be mentioned as an example; as agro-industrial residue, it has already been used as a source of silica for the synthesis of catalysts applied in the degradation of terephthalate acid [20] and discoloration of methyl violet dye [21].

Some quarries generate, in excess volumes, a by-product called stone powder or rock powder. This material has characteristics and chemical composition that varies and depends on the type of rock to be explored. In intrusive igneous rocks, silicon dioxide (SiO_2) is one of the most significant components and the classification of the rock occurs according to the SiO_2 present amount: above 63% are acid igneous rocks, 52–63% are intermediate or neutral igneous rocks, 45–52% are mafic or basic igneous rocks, and <45% are ultramafic or ultrabasic igneous rocks [22]. Using this type of in-water treatment waste is a recent and promising proposal.

In this context, the present work contributes with a new material catalytic/adsorbent material, giving value a residue, as an alternative to traditional catalysts/adsorbent (mineral by-product). In addition, tests with industrial effluent, from the packaging industry, samples were collected for a period of seven consecutive days, considering the industrial process dynamics. The photocatalytic and adsorptive capacity of the stone powder was evaluated in the discoloration, applied both to the synthetic effluent and to the industrial effluent.

2. Results and Discussion

2.1. Catalysts Characterizations

Figure 1 shows the results for SEM-EDS, PAS, and XRD for ZnO and the mineral by-product (MbP).

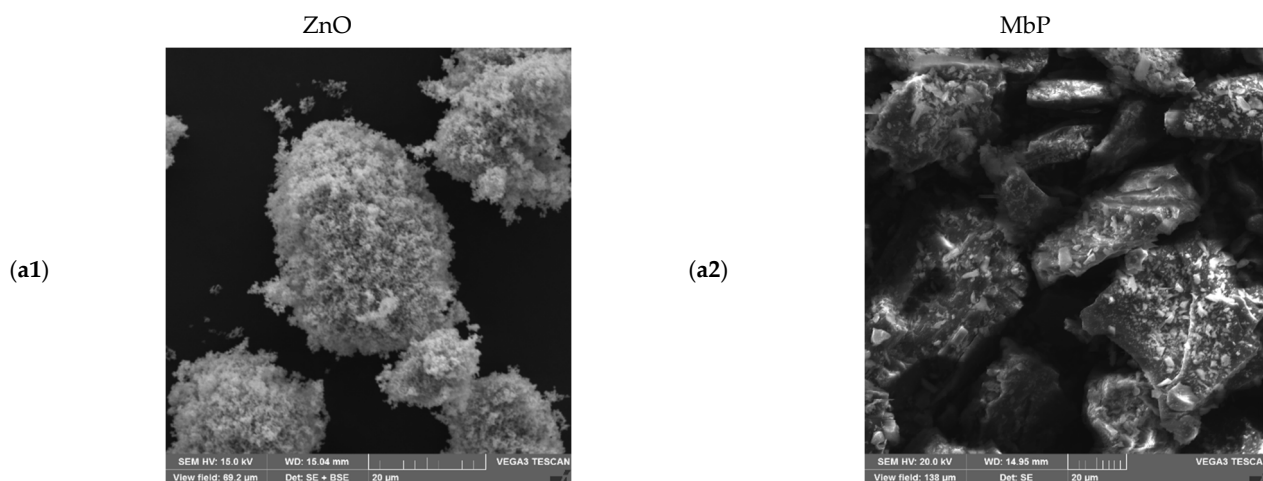


Figure 1. Conts.

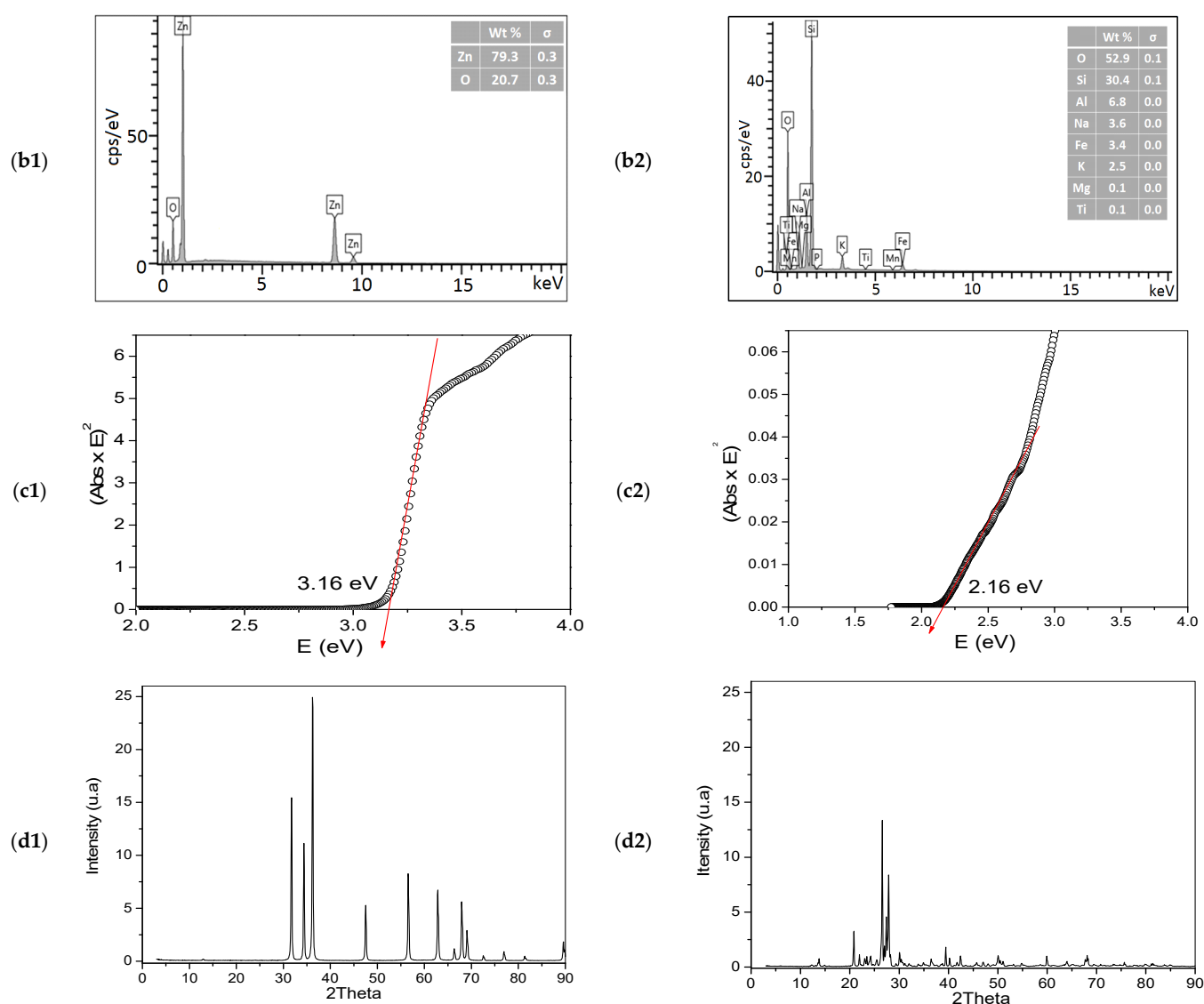


Figure 1. Characterizations of ZnO and mineral by-product (MbP): (a1,b1,c1) and (d1) correspond to SEM, EDS, PAS and XRD to ZnO, respectively. And (a2,b2,c2) and (d2) correspond to SEM, EDS, PAS and XRD to MbP, respectively.

The ZnO composition is defined by approximately 80% zinc and 20% oxygen (Figure 1), the material bandgap energy is 3.16 eV, and a crystalline definition in hexagonal wurtzite, which is the most common for this material. Such characteristics are similar to those already described in the literature [23–25].

For the MbP, there is a large number of elements in its structure; however, the elements O, Si, and Al correspond to approximately 90% of the material. In this way, is possible to compare the quarry residue used with quartz sand, which is also naturally composed of silica and other impurities such as Fe₂O₃, Al₂O₃, TiO₂, CaO, MgO, and K₂O [24]. Materials containing silica (SiO₂) and alumina (Al₂O₃) can be found in the literature as supporting materials for catalysts [26,27]. Regarding the MbP crystallinity, the peaks identified in 2 θ between 20 and 30° is characteristic of the hexagonal mesoporous silicate [28]; in addition, the MbP E_{gap} value was close to 2.16 eV, being very close to E_{gap} of Si nanoparticles from quartz sand, defined at 2.22 eV [29].

2.2. Experimental Tests

PH and Catalyst Concentration

The experimental tests first carried out were aimed at identifying the optimal parameters, pH, and catalyst/adsorbent concentration for both industrial and synthetic effluents. Figures 2 and 3 indicate the results obtained for synthetic and industrial effluent and material used. All graphs referring to the experimental tests are presented as C/C_0 versus time (min), where C (mg L^{-1}) is the concentration at any time t (min), and C_0 is the initial concentration ($t = 0$).

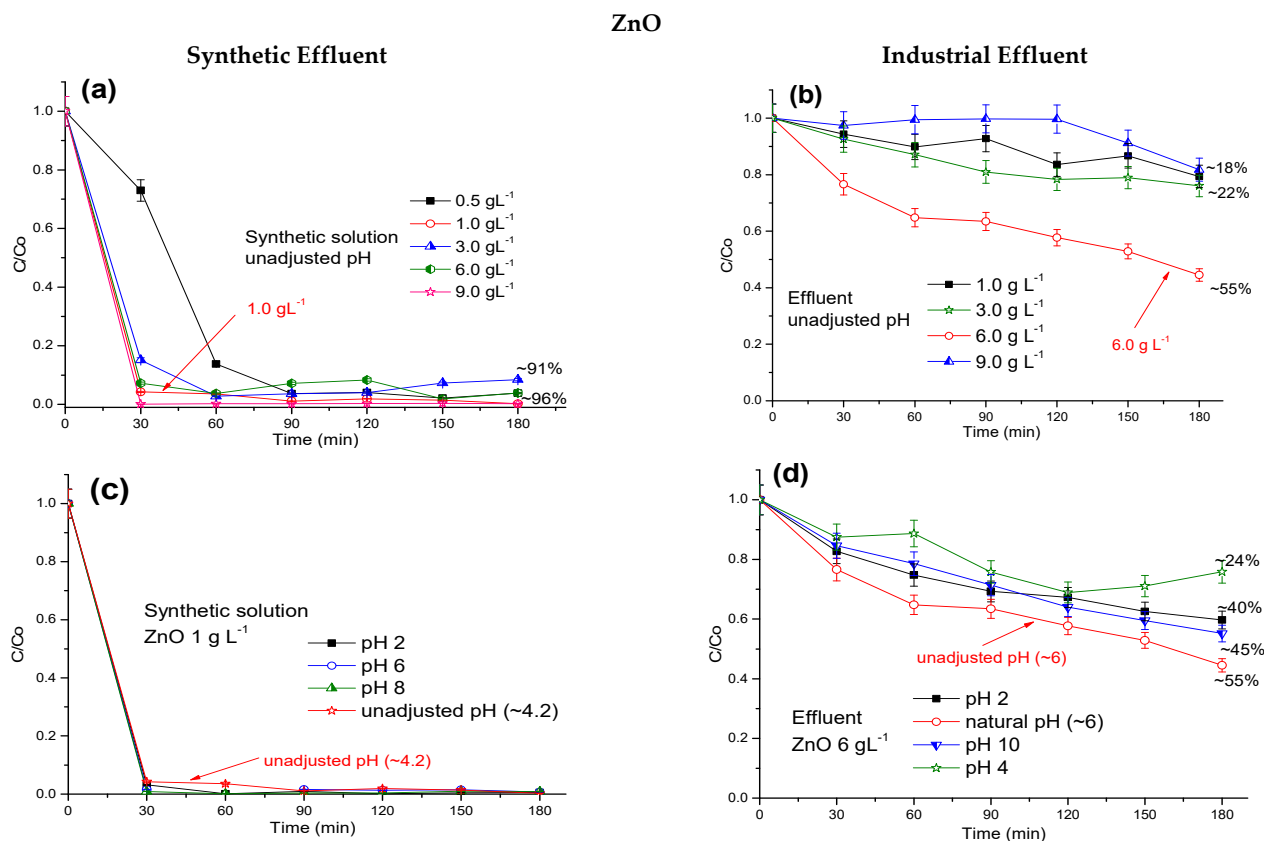


Figure 2. Catalyst concentration (a,b) and pH (c,d) tests for ZnO with synthetic and industrial effluent.

Figures 2 and 3 have some aspects in common that can be highlighted; for example, when the industrial effluent was treated, there was a greater and faster solution discoloration. This fact is related to the effluent composition, that is, while the synthetic effluent contained only dye and distilled water, the industrial effluent had a large organic load. Figure 7 indicated that the presence of organic compounds can impair photocatalytic reactions since such compounds will compete for surface adsorption with the material's active sites.

Another aspect that can be highlighted is that the catalyst concentration has also been changed independently of the used material. When the photocatalytic process was applied in the synthetic effluent, 1.0 g L^{-1} was the solution was satisfactorily discolored; on the other hand, for the industrial effluent, 6.0 g L^{-1} was needed so that greater percentages of discoloration were achieved.

Although with MbP in the 9.0 g L^{-1} concentration, at the beginning of the reaction, it had a quick discoloration, the difference for when 6.0 g L^{-1} was used was small; thus, this would not justify an increase of 50% in catalyst concentration for the reaction.

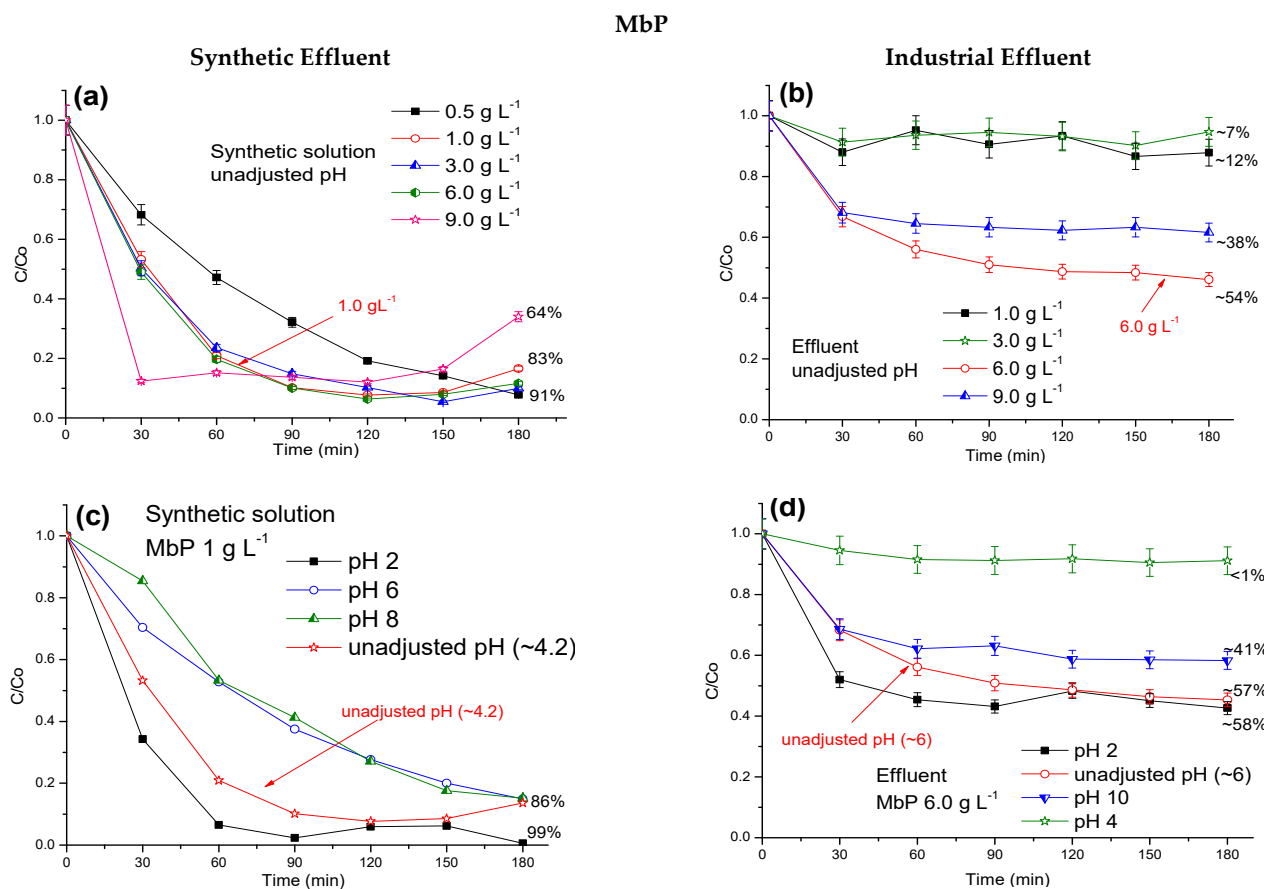


Figure 3. Catalyst concentration (a,b) and pH (c,d) tests for MbP with synthetic and industrial effluent.

The reaction speed is related to the photocatalyst concentration. As the concentration of catalysts increases, reaction speed is increased, as more active sites will be available. However, when this concentration reaches an optimum point, if more photocatalyst is added, the reaction may be impaired, and therefore, radiation penetration tends to decrease with the light screening effect, a factor often observed by different authors with different pollutants [30–32].

Regarding the pH of the reaction medium, for both cases, it appears that the pH without adjustment, that is, the unadjusted pH proper to the effluent (synthetic ~4.2 or industrial ~6.2) were identified as ideal for photoreaction.

The working advantage with the solution itself, that is, without adjustments, is the time that is saved in the adjustment steps before and after reactions. Figure 4 shows the results obtained for photolysis and adsorption tests (synthetic solution).

Both photolysis and adsorption results demonstrate the need for a photocatalyst-radiation combination for greater discoloration of the synthetic solution.

After defining the pH and catalyst concentration conditions, i.e., pH without adjustment (unadjusted pH) and 6.0 g L^{-1} of ZnO or MbP, the experimental tests were realized for samples collected from the industrial effluent during seven consecutive days.

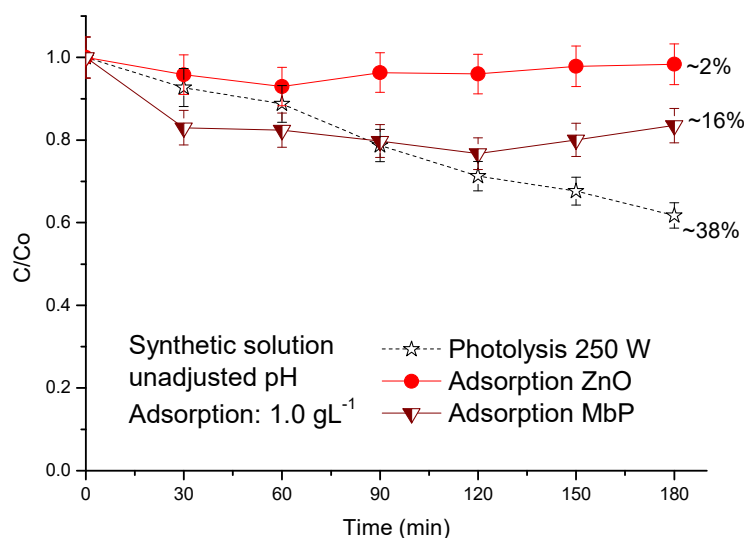


Figure 4. Photolysis and adsorption with synthetic solution, unadjusted pH, and concentration of 1 gL^{-1} of ZnO or MbP.

2.3. Industrial Effluent

Molded pulp packaging, which is the product manufactured in the company where the industrial effluent was collected, is basically made of paper, water, and additives, and follows a process, as described in Figure 5.

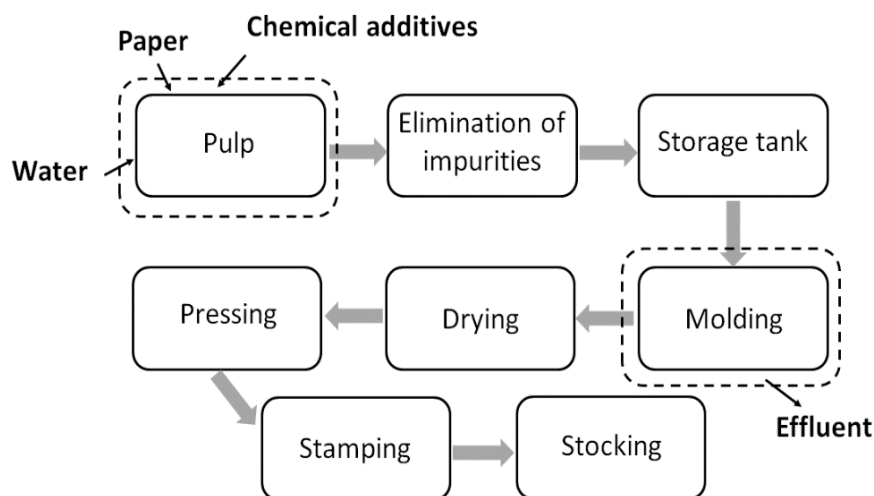


Figure 5. The manufacturing process of molded pulp packaging.

The first stage of the process is the formation of the pulp, which consists of water, chemical additives, and paper of different types; then, this pulp undergoes a process in which the gross impurities are removed. Subsequently, the mass proceeds to a storage tank that feeds the equipment used for molding, which basically consists of pressure and suction operations of excess water. Then, the ready packages are processed, by means of mats, for drying which, depending on the moisture conditions of the material, are heated from 180 to $240 \text{ }^\circ\text{C}$ for approximately 10 to 15 min and, finally, before advancing to the printing (the step in which it adds images and writings according to what was established by the client), the packages undergo a pressing process in which the objective is to provide a better finish and resistance [33].

Currently, the effluent that leaves the molding stage is reused without being subjected to any treatment at the inputs entrance for the pulp manufacture. However, it is very difficult to adjust the color of the next batch of packaging, since in some cases, other dyes are also used. This situation causes dissatisfaction among customers, as there is no color standardization. Therefore, based on the results we had in item 2.2, the effluent treatment was realized, aiming to identify the parameter variation and how the reactions would be conducted. Figure 6 shows the results.

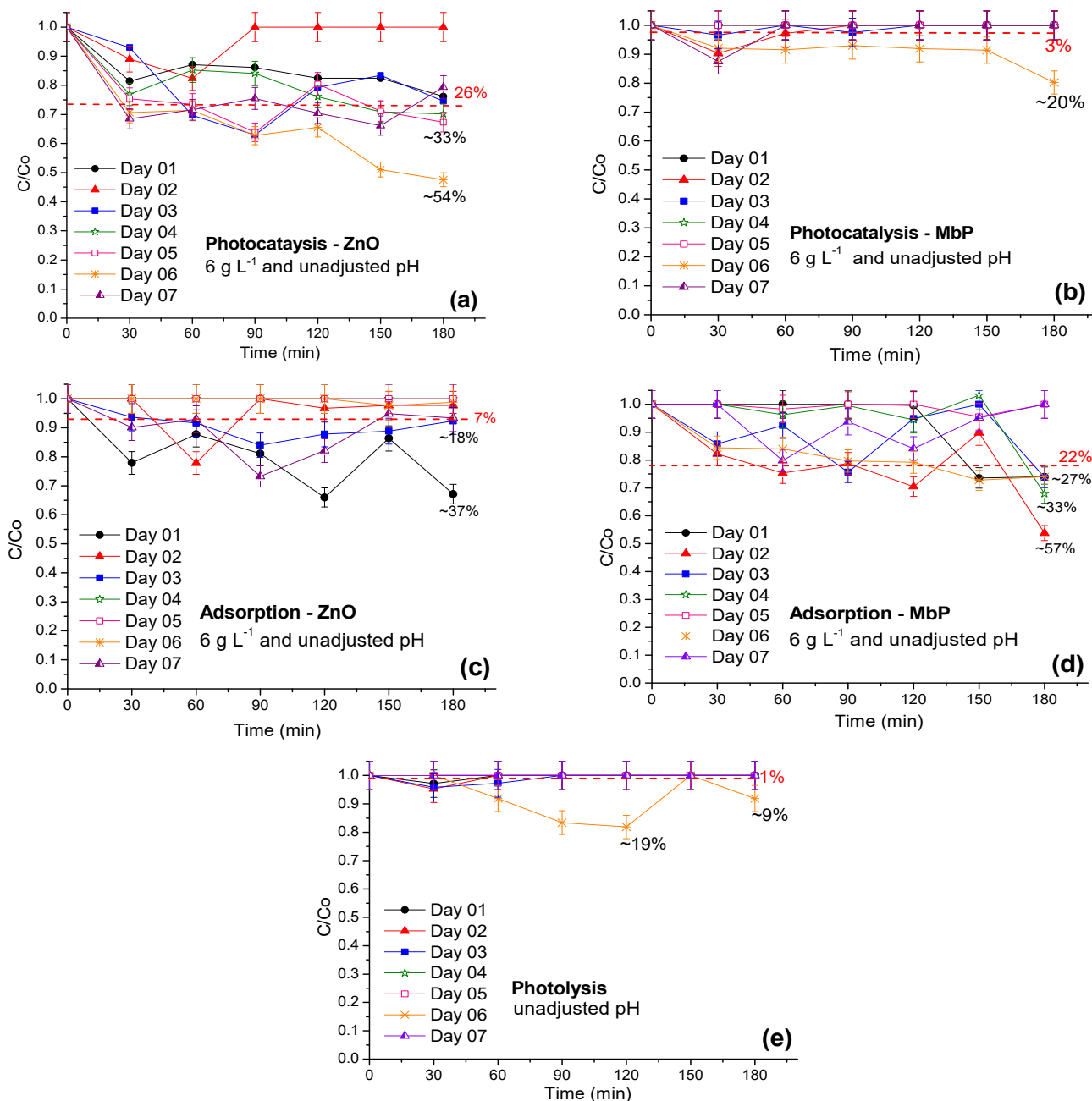


Figure 6. Tests of heterogeneous photocatalysis (a,b), adsorption (c,d), and photolysis (e) of industrial effluents.

Figure 7 shows the initial composition of each collected effluent sample and its subsequent composition after the reactions used. The variables total soluble solids and N (NO₃); surfactants are not quantified in the graph since they always presented the same values of <100, <10, and <10, respectively.

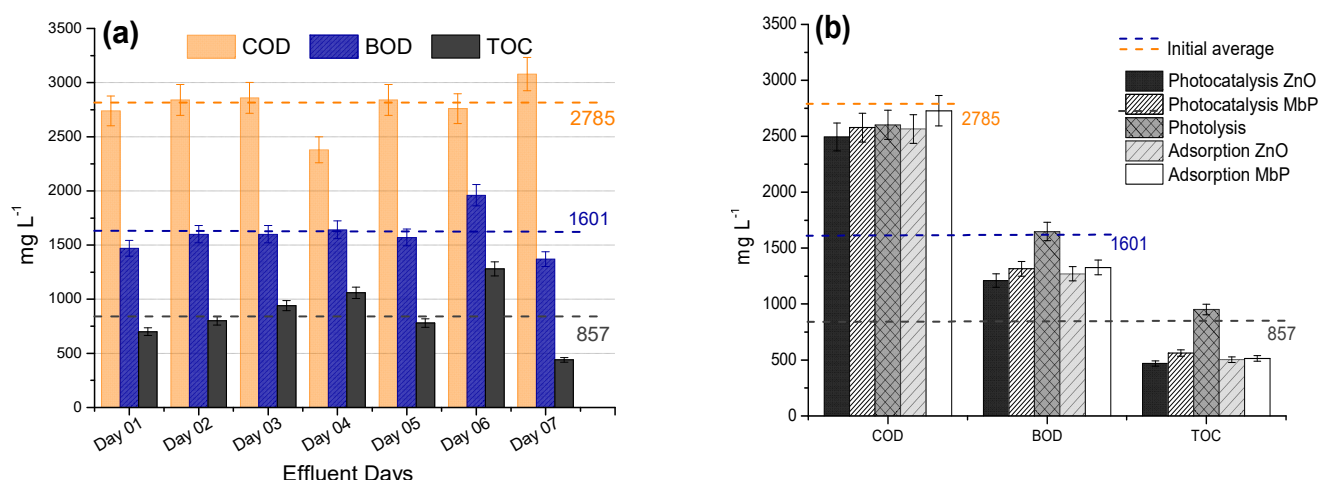


Figure 7. Organic load (a) initially and (b) after reactions with industrial effluents. The dashed lines indicate the initial average of COD, BOD, and TOC (mg L^{-1}) of the 7 days from the collected effluent.

There was great variation in the efficiency of the tests performed, beginning with the photocatalytic tests that showed an average of 26% and 3% discoloration when used ZnO and MbP, respectively, which is a significant drop when compared to the results shown in Figures 3 and 4. Photolysis had unfavorable performance, both in the discoloration of the dye (Figure 6e) and in the organic load reduction (Figure 7b). Regarding adsorption, it appears that MbP was, generally, a good adsorbent of the present dye in the industrial effluent, presenting on average 22%.

All this unstable behavior observed during the reactions is related to the variation in the industrial effluent composition observed in Figure 7a. Changes in the reactions kinetic behavior when using a synthetic dye solution and when using an industrial effluent have already been observed in the literature [34] in which the authors evaluated the discoloration of synthetic effluent containing blue dye and industrial textile effluent and verified a decrease in the efficiency of the process when industrial textile effluent was used. In the literature [35], they also verified superior results when they treated a synthetic effluent containing dye rather than real industrial effluent. Both authors justified this behavior due to the effluent's composition, such as the presence of interfering ions and organic load.

Organic compounds, when present in the solution, can compete for the photogenerated hydroxyl radical and the active sites available on the catalyst surface with the target pollutant, which, in the present research, was the dye CI basic yellow 96, which can decrease the efficiency of photocatalysis [36].

When comparing the initial composition of this effluent with other effluents already studied, it can be highlighted that the effluent from the molded pulp packaging industry has a high organic load with high values of COD, BOD, and TOC when compared with other effluents, as reported in the literature [37,38].

In addition to the concentration reduction of dye present in the effluent, it is necessary to evaluate the organic load decrease. It is noted that for all reactions, except for the photolysis reactions, a decrease in the organic load occurs, mainly in terms of TOC. This parameter (TOC) is related to the pollutant mineralization; in the present study, it is possible to notice that the dye degradation and the mineralization of the same occurred simultaneously [39,40]. It is important to note that adsorption has also been shown to be effective in reducing organic matter. The decrease in organic load in the industrial effluent brings benefits to the water quality since the organic load has less capacity to pollute the effluent.

In the present work, it is possible to affirm that MbP has catalytic properties; however, it also presented an adsorbent behavior in some experimental tests. MbP is a low-cost material available in large quantities, which can bring financial benefits to the companies involved. Quartz sand, which is a material very similar to the by-product studied in the present work, has also been applied as an adsorbent and has shown promising results such

as the methylene blue dye adsorption [41], together with graphene in the adsorption of Hg^{2+} e Pb^{2+} [42] and the adsorption of Ciprofloxacin [43].

Using waste or by-products as catalysts is a recent proposal and involves numerous challenges. Some authors have already described the performance of residues as catalysts and adsorbents in the most diverse degradations and adsorption, such as, for example, the study [44], in which they studied the use of depleted acacia bark (agro-industrial waste) as support for photocatalysts used in the degradation of organic phenolic pollutants, and the study [45], in which they used bauxite residue from the aluminum industry as a new photocatalyst for hydrogen generation. However, in most research studies, the photocatalytic reactions use the residues only as a support for catalysts such as TiO_2 or else as a source of some metal to be impregnated in the semiconductor. Studies are carried out with pollutants present in synthetic solutions, which facilitate the reproducibility of the results and applicability favor the new catalyst.

3. Materials and Methods

3.1. Chemicals

The used dye in the synthetic solution reactions was supplied by the same company that supplied the real effluent; this dye is known as CI Basic Yellow 96 (BASF–Solenis), is used to dye the molded pulp packaging in industrial processes, has a yellow color, and liquid form.

The materials used as catalysts and adsorbents were (i) zinc oxide (ZnO) as a reference material, supplied by Dinâmica Química Ltd.a (Sao Paulo, Brazil) and (ii) quarry residue, in this work defined as a mineral by-product (MbP).

The MbP was supplied by a company located in the region of Campos Gerais in the state of Paraná—Brazil. This company operates in the sale of stones and gravel, asphalt, providing services in the area of earthworks and paving. The rock explored is classified as intrusive igneous granite. Both ZnO and MbP were used without previous treatment; however, their grain size was standardized. Both were sieved in order to obtain particles smaller than 0.3 mm. This characteristic is observed in the ZnO (used as a reference).

3.2. Catalysts Characterizations

3.2.1. Scanning Electron Microscopy (SEM) Associated with Dispersive Energy Spectroscopy (EDS)

Samples were metalized with gold using IC-50 ION COATER (Shimadzu) for 10 min. The topographic surface images were obtained using a scanning electron microscope model VEGA 3 LMU brand TESCAN, complete with, 30 kV W filament, 3.0 nm resolution, retractable SE and BSE detectors, low-vacuum mode (500 Pa) chamber with an internal diameter of 230 mm, and a CCD camera for viewing the sample chamber. The microscope is also equipped with EDS Detector, model AZTec Energy X-Act, resolution 130 eV, brand Oxford.

3.2.2. X-ray Diffraction (XRD)

A Bruker D8 Advance X-ray diffractometer, 2θ from 5 to 80° , with $2^\circ/\text{min}$ in the scan, 40 kV and 35 mA was used. The result obtained was then analyzed using standards published by the International Center for Diffraction Data (ICDD).

3.2.3. Photoacoustic Spectroscopy (PAS)

A source with Xenon lamp emitted a light that passed through a monochromator, (Oriel, model 66,936 (1/4 m), with inlet and outlet slits adjusted to 3.00 mm. The frequency of light modulation was controlled by a mechanical modulator (Stanford Research Systems, model SR 540) which, with a photodiode, provided a reference signal for the amplifier (lock-in). The microphone attached to the photoacoustic cell (Brüel & Kjaer, model BK 4953) was connected to a power source and a preamplifier. The microphone signal was transferred to a synchronized amplifier (EG & G Instruments, model 5110), and the amplifier provided intensity, and the phase of the photoacoustic signal was transferred to a personal computer;

the spectra (modulation frequency 23 Hz) were normalized with respect to the carbon signal. Direct bandgap energy (E_{gap}) was acquired from a linear fit in the graph obtained from the square of the absorption coefficient ($(\text{Abs} \times (1240/\lambda))^2$) as a function of photon energy (E) ($1240/\lambda$) [25,41].

3.3. Experimental Tests

The synthetic effluents were prepared with distilled water with a dye concentration of $10 \mu\text{L L}^{-1}$, and industrial effluents were supplied by the molded pulp packaging.

The experimental tests were carried out in a jacketed borosilicate reactor (cooling water temperature $13 \text{ }^\circ\text{C}$) to maintain the effluent temperature at approximately $25 \text{ }^\circ\text{C}$; the nominal volume was 600 mL, and 500 mL of effluent (artificial or industrial) was used for the reactions. The system contained a mercury vapor lamp (250 W), coupled just above the reactor, that was open to the environment. Magnetic stirring and air bubbling (0.5 L min^{-1}) into the reaction medium were used. During the reaction, samples were collected, centrifuged, and the dye residual concentration was analyzed in a UV-Vis spectrophotometer (Femto-800 XI) with a wavelength of 429 nm, dye characteristic.

The photolysis tests followed the same reaction system, but without the presence of airflow and catalyst, to verify only the radiation action under the discoloration reaction. The adsorption tests were realized without radiation and airflow to verify the adsorptive capacity of the studied materials.

3.3.1. pH and Catalyst Concentration Influence

For the pH tests, NaOH and HCl solutions were used for the adjustments, and the values were adjusted between 2 and 10; in addition, tests were also carried out without pH adjustment (unadjusted pH): synthetic effluent ~ 4.2 and industrial effluent ~ 6.2 . For the catalyst concentration optimization, values between 0.5 and 9 g L^{-1} were evaluated. Both tests were carried out with artificial and industrial effluent preceding the tests carried out for one week.

3.3.2. Industrial Effluent—Treatment for One Week

After the conditions (pH and catalyst concentration) were defined, adsorption, photolysis, and photocatalytic tests were carried out for one week (seven days) to treat the industrial effluent provided by the molded pulp packaging industry. Every day, the effluent was collected immediately at the molded outlet and then transported to the laboratory where the tests were carried out in parallel, following the same conditions described in item 2.3. Industrial effluents were subjected to experimental tests as they were received, without previous treatment.

3.4. Characterization of Industrial Effluent

The effluent was characterized quantitatively, identifying and comparing the parameters before and after each reaction. The analyzed parameters were biological oxygen demand (BOD), chemical oxygen demand (COD), total organic carbon (TOC), total soluble solids (TSS), surfactants, and nitrogen–nitrate $\text{N}(\text{NO}_3)$. The characterization was performed on the Pastel UV-Secomam equipment, with all analyses performed in duplicates.

This equipment determines the quality of the water and effluents. The method is based on spectral deconvolution where the ultraviolet spectrum hypothesis of effluents can be mostly modeled by a limited number of stable spectrums called the reference spectrum. Many studies have already used it to determine the quality of the effluents [42–45].

4. Conclusions

The use of photocatalysts resulting from industrial waste in the effluents' treatment is favorable. However, factors such as the composition variation of the material and the pollutant should be considered, mainly because when it comes to industrial effluents, it is difficult to identify a pattern. In this research, it was found that a quarry by-product

has similar characteristics quartz sand, which is a material already used as a catalyst support and also as an adsorbent for organic pollutants. It was noted that the material has catalytic activity when used as a photocatalyst, showing behavior favorable for synthetic dye solutions. However, when applied to the industrial effluent discoloration from the packaging industry, with a high organic load, it presented better behavior, in most tests, as an adsorbent. Although it has shown lower results than ZnO, MbP can be considered a promising material in the treatment of aqueous solutions.

Author Contributions: Conceptualization, L.N.B.d.A.; T.G.J. and G.G.L., methodology, L.N.B.d.A.; T.G.J.; O.H.L.N. and G.G.L. validation, L.N.B.d.A.; T.G.J.; A.M.T. and G.G.L., formal analysis, G.G.L.; A.M.T.; O.A.A.d.S. and D.T.D., investigation L.N.B.d.A.; T.G.J.; O.H.L.N.; A.M.T. and G.G.L., data curation, L.N.B.d.A.; G.G.L. and A.M.T., writing—original draft preparation, L.N.B.d.A.; T.G.J. and G.G.L., writing—review and editing, L.N.B.d.A.; T.G.J., D.T.D. and G.G.L., visualization, L.N.B.d.A.; T.G.J. and G.G.L., supervision, G.G.L. and O.A.A.d.S., project administration, L.N.B.d.A.; G.G.L. and O.A.A.d.S. All authors have read and agreed to the published version of the manuscript.

Funding: This research received no external funding.

Acknowledgments: The authors would like to thank the CNPq and CAPES for the financial support, UEM, and Multi-User Characterization Center in Materials Research and Development (C2MMA) for analyzes carried. This research did not receive any specific grant from funding agencies in the public, commercial, or not-for-profit sectors.

Conflicts of Interest: The authors declare no conflict of interest.

References

1. Santos, D.H.; Duarte, J.L.; Tavares, M.G.; Tavares, M.G.; Friedrich, L.C.; Meili, L.; Pimentel, W.R.; Tonholo, J.; Zanta, C.L. Electrochemical degradation and toxicity evaluation of reactive dyes mixture and real textile effluent over DSA[®] electrodes. *Chem. Eng. Process. Intensif.* **2020**, *153*, 107940. [[CrossRef](#)]
2. Ismail, M.; Wu, Z.; Zhang, L.; Ma, J.; Jia, Y.; Hu, Y.; Wang, Y. High—Efficient synergy of piezocatalysis and photocatalysis in bismuth oxychloride nanomaterial for dye decomposition. *Chemosphere* **2019**, *228*, 212–218. [[CrossRef](#)] [[PubMed](#)]
3. Dil, E.A.; Ghaedi, M.; Asfaram, A.; Mehrabi, F.; Sadeghfar, F. Efficient adsorption of Azure B onto CNTs/Zn:ZnO@Ni2P-NCs from aqueous solution in the presence of ultrasound wave based on multivariate optimization. *J. Ind. Eng. Chem.* **2019**, *74*, 55–62. [[CrossRef](#)]
4. Wu, S.; Xie, Y.; Zhang, X.; Huang, Z.; Liu, Y.; Fang, M.; Wu, X.; Min, X. In situ synthesis of adsorptive β -Bi2O3/BiOBr photocatalyst with enhanced degradation efficiency. *J. Mater. Res.* **2019**, *34*, 3450–3461. [[CrossRef](#)]
5. Riaz, S.; Park, S.-J. An overview of TiO2-based photocatalytic membrane reactors for water and wastewater treatments. *J. Ind. Eng. Chem.* **2020**, *84*, 23–41. [[CrossRef](#)]
6. Josué, T.; Almeida, L.; Lopes, M.; Santos, O.; Lenzi, G. Cr (VI) reduction by photocatalytic process: Nb2O5 an alternative catalyst. *J. Environ. Manag.* **2020**, *268*, 110711. [[CrossRef](#)]
7. Lenzi, G.; Favero, C.V.B.; Colpini, L.; Bernabe, H.; Baesso, M.; Specchia, S.; Santos, O. Photocatalytic reduction of Hg(II) on TiO2 and Ag/TiO2 prepared by the sol–gel and impregnation methods. *Desalination* **2011**, *270*, 241–247. [[CrossRef](#)]
8. Almeida, L.; Lenzi, G.; Pietrobelli, J.; Santos, O. Caffeine degradation using ZnO and Ag/ZnO under UV and solar radiation. *Desalination Water Treat.* **2019**, *153*, 85–94. [[CrossRef](#)]
9. Sornalingam, K.; McDonagh, A.; Canning, J.; Cook, K.; Johir, A.H.; Zhou, J.L.; Ahmed, M.B. Photocatalysis of 17 α -ethynylestradiol and estriol in water using engineered immersible optical fibres and light emitting diodes. *J. Water Process. Eng.* **2020**, *33*, 101075. [[CrossRef](#)]
10. Chen, P.; Blaney, L.; Cagnetta, G.; Huang, J.; Wang, B.; Wang, Y.; Deng, S.; Yu, G. Degradation of Ofloxacin by Perylene Diimide Supramolecular Nanofiber Sunlight-Driven Photocatalysis. *Environ. Sci. Technol.* **2019**, *53*, 1564–1575. [[CrossRef](#)]
11. Tiwari, D.; Tiwari, A.; Shukla, A.; Kim, D.J.; Yoon, Y.Y.; Lee, S.M. Facile synthesis and characterization of nanocomposite Au0(NPs)/titanium dioxide: Photocatalytic degradation of Alizarin Yellow. *J. Ind. Eng. Chem.* **2020**, *82*, 153–163. [[CrossRef](#)]
12. Morais, D.F.; Boaventura, R.A.; Moreira, F.C.; Vilar, V.J. Bromate removal from water intended for human consumption by heterogeneous photocatalysis: Effect of major dissolved water constituents. *Chemosphere* **2021**, *263*, 128111. [[CrossRef](#)]
13. Litter, M. *Treatment of Chromium, Mercury, Lead, Uranium, and Arsenic in Water by Heterogeneous Photocatalysis*, 1st ed.; Elsevier BV: Amsterdam, The Netherlands, 2009. [[CrossRef](#)]
14. Zhao, T.; Qian, R.; Zhou, G.; Wang, Y.; Lee, W.I.; Pan, J.H. Mesoporous WO3/TiO2 spheres with tailored surface properties for concurrent solar photocatalysis and membrane filtration. *Chemosphere* **2021**, *263*, 128344. [[CrossRef](#)] [[PubMed](#)]
15. Chen, D.; Cheng, Y.; Zhou, N.; Chen, P.; Wang, Y.; Li, K.; Huo, S.; Cheng, P.; Peng, P.; Zhang, R.; et al. Photocatalytic degradation of organic pollutants using TiO2-based photocatalysts: A review. *J. Clean. Prod.* **2020**, *268*, 121725. [[CrossRef](#)]

16. Gonçalves, B.S.; Silva, L.M.; de Souza, T.C.; de Castro, V.G.; Silva, G.G.; Silva, B.C.; Krambrock, K.; Soares, R.B.; Lins, V.F.; Houmard, M.; et al. Solvent effect on the structure and photocatalytic behavior of TiO₂-RGO nanocomposites. *J. Mater. Res.* **2019**, *34*, 3918–3930. [[CrossRef](#)]
17. Liu, S.; Wang, Y.; Ma, L.; Zhang, H. Ni₂P/ZnS (CdS) core/shell composites with their photocatalytic performance. *J. Mater. Res.* **2018**, *33*, 3580–3588. [[CrossRef](#)]
18. Kako, T.; Yao, W.; Ye, J. Preparation and characterization of visible light sensitive Fe- and Ta-codoped TiO₂ photocatalyst. *J. Mater. Res.* **2010**, *25*, 110–116. [[CrossRef](#)]
19. Fu, Y.P.; Chang, W.K.; Wang, H.C.; Liu, C.W.; Lin, C.H. Synthesis and characterization of anatase TiO₂ nanolayer coating on Ni–Cu–Zn ferrite powders for magnetic photocatalyst. *J. Mater. Res.* **2010**, *25*, 134–140. [[CrossRef](#)]
20. Yener, H.B.; Helvacı, Ş.Ş. Effect of synthesis temperature on the structural properties and photocatalytic activity of TiO₂/SiO₂ composites synthesized using rice husk ash as a SiO₂ source. *Sep. Purif. Technol.* **2015**, *140*, 84–93. [[CrossRef](#)]
21. Fatimah, I.; Said, A.; Hasanah, U.A. Preparation of TiO₂-SiO₂ using Rice Husk Ash as Silica Source and The Kinetics Study as Photocatalyst in Methyl Violet Decolorization. *Bull. Chem. React. Eng. Catal.* **2015**, *10*, 43–49. [[CrossRef](#)]
22. Haldar, S.K. Igneous rocks. In *Introduction to Mineralogy and Petrology*, 2nd ed.; Elsevier: Amsterdam, The Netherlands, 2014; pp. 159–186. [[CrossRef](#)]
23. Mills, A.; Davies, R.H.; Worsley, D. Water Purification by Semiconductor Photocatalysis. *Chem. Soc. Rev.* **2010**, *25*, 417–425. [[CrossRef](#)]
24. Abebe, B.; Murthy, H.A.; Amare, E. Enhancing the photocatalytic efficiency of ZnO: Defects, heterojunction, and optimization. *Environ. Nanotechnol. Monit. Manag.* **2020**, *14*, 100336. [[CrossRef](#)]
25. Sa-Nguanprang, S.; Phuruangrat, A.; Thongtem, T.; Thongtem, S. Characterization and photocatalysis of visible-light-driven Dy-doped ZnO nanoparticles synthesized by tartaric acid-assisted combustion method. *Inorg. Chem. Commun.* **2020**, *117*, 107944. [[CrossRef](#)]
26. Garbarino, G.; Phung, T.K.; Pampararo, G.; Riani, P.; Busca, G. Modification of the properties of γ—Alumina as a support for nickel and molybdate catalysts by addition of silica. *Catal. Today* **2021**. [[CrossRef](#)]
27. Park, J.L.; Canizales, K.A.; Argyle, M.D.; Woodfield, B.F.; Stowers, K.J. The effects of doping alumina with silica in alumina-supported NiO catalysts for oxidative dehydrogenation of ethane. *Microporous Mesoporous Mater.* **2020**, *293*, 109799. [[CrossRef](#)]
28. Farjadian, F.; Azadi, S.; Mohammadi-Samani, S.; Ashrafi, H.; Azadi, A. A novel approach to the application of hexagonal mesoporous silica in solid-phase extraction of drugs. *Heliyon* **2018**, *4*, e00930. [[CrossRef](#)]
29. Arunmetha, S.; Vinoth, M.; Srither, S.R.; Karthik, A.; Sridharpanday, M.; Suriyaprabha, P.; Manivasakan, R.; Rajendran, V. Study on Production of Silicon Nanoparticles from Quartz Sand for Hybrid Solar Cell Applications. *J. Electron. Mater.* **2017**, *47*, 493–502. [[CrossRef](#)]
30. Mangrulkar, P.A.; Kamble, S.P.; Joshi, M.M.; Meshram, J.S.; Labhsetwar, N.K.; Rayalu, S.S. Photocatalytic Degradation of Phenolics by N-Doped Mesoporous Titania under Solar Radiation. *Int. J. Photoenergy* **2011**, *2012*, 1–10. [[CrossRef](#)]
31. Taffarel, S.R.; Lansarin, M.A.; Moro, C. Styrene photocatalytic degradation reaction kinetics. *J. Braz. Chem. Soc.* **2011**, *22*, 1872–1879. [[CrossRef](#)]
32. Wetchakun, K.; Wetchakun, N.; Sakulsermsuk, S. An overview of solar/visible Light—Driven heterogeneous photocatalysis for water purification: TiO₂- and ZnO-based photocatalysts used in suspension photoreactors. *J. Ind. Eng. Chem.* **2019**, *71*, 19–49. [[CrossRef](#)]
33. Martínez, K.Y.P.; Toso, E.A.V. Planejamento da produção na indústria de embalagens de polpa moldada. *Gestão Produção* **2014**, *23*, 649–660. [[CrossRef](#)]
34. Jada, A.; Akbour, R.A. Adsorption and Removal of Organic Dye at Quartz Sand-Water Interface. *Oil Gas Sci. Technol.* **2014**, *69*, 405–413. [[CrossRef](#)]
35. Ceretta, M.B.; Vieira, Y.; Wolski, E.A.; Foletto, E.L.; Silvestri, S. Biological degradation coupled to photocatalysis by ZnO/polypyrrole composite for the treatment of real textile wastewater. *J. Water Process. Eng.* **2020**, *35*, 101230. [[CrossRef](#)]
36. Garcia, V.S.; Rosa, J.M.; Borrelly, S.I. Toxicity and color reduction of a textile effluent containing reactive red 239 dye by electron beam irradiation. *Radiat. Phys. Chem.* **2020**, *172*, 108765. [[CrossRef](#)]
37. Nguyen, C.H.; Juang, R.-S. Efficient removal of cationic dyes from water by a combined adsorption-photocatalysis process using Platinum—Doped titanate nanomaterials. *J. Taiwan Inst. Chem. Eng.* **2019**, *99*, 166–179. [[CrossRef](#)]
38. Ma, J.; Wang, K.; Wang, C.; Chen, X.; Zhu, W.; Zhu, G.; Yao, W.; Zhu, Y. Photocatalysis-self-Fenton system with high-fluent degradation and high mineralization ability. *Appl. Catal. B Environ.* **2020**, *276*, 119150. [[CrossRef](#)]
39. Mohammad-Rezaei, R.; Jaymand, M. Graphene quantum dots coated on quartz sand as efficient and low-cost adsorbent for removal of Hg²⁺ and Pb²⁺ from aqueous solutions. *Environ. Prog. Sustain. Energy* **2018**, *38*, S24–S31. [[CrossRef](#)]
40. Xu, X.; He, J.; Li, Y.; Fang, Z.; Xu, S. Adsorption and Transport of Ciprofloxacin in Quartz Sand at Different pH and Ionic Strength. *Open J. Soil Sci.* **2014**, *04*, 407–416. [[CrossRef](#)]
41. Astrath, N.G.C.; Sato, F.; Pedrochi, F.; Medina, A.N.; Bento, A.C.; Baesso, M.L.; Persson, C.; Da Silva, A.F. Band gap energy determination by photoacoustic spectroscopy under continuous light excitation. *Appl. Phys. Lett.* **2006**, *89*, 231926. [[CrossRef](#)]
42. Ito, T.; Shimada, Y.; Suto, T. Potential use of bacteria collected from human hands for textile dye decolorization. *Water Resour. Ind.* **2018**, *20*, 46–53. [[CrossRef](#)]

43. Methneni, N.; Morales-González, J.A.; Jaziri, A.; Ben Mansour, H.; Fernandez-Serrano, M. Persistent organic and inorganic pollutants in the effluents from the textile dyeing industries: Ecotoxicology appraisal via a battery of biotests. *Environ. Res.* **2021**, *196*, 110956. [[CrossRef](#)] [[PubMed](#)]
44. Adamczuk, M.; Pawlik-Skowrońska, B.; Solis, M. Do anthropogenic hydrological alterations in shallow lakes affect the dynamics of plankton? *Ecol. Indic.* **2020**, *114*, 106312. [[CrossRef](#)]
45. Mieczan, T.; Rudyk-Leuska, N. Seasonal dynamics of the epibiont food web on *Unio tumidus* (Philipsson, 1788) in a eutrophic reservoir. *Eur. J. Protistol.* **2019**, *69*, 138–150. [[CrossRef](#)] [[PubMed](#)]